PROCEEDINGS of the
23rd International Congress on Acoustics

9 to 13 September 2019 in Aachen, Germany

On the effects of leading edge serrations on aeroacoustic properties during stall

Yannick D. Mayer*, B. Zang†, Mahdi Azarpeyvand‡

Faculty of Engineering, University of Bristol, United Kingdom

ABSTRACT

The effect of leading edge serrations on the surface pressure fluctuation spectra and boundary layer quantities of a NACA 0012 airfoil has been investigated experimentally, with an emphasis on reducing airfoil separation and stall noise. Five leading edge serration add-ons with various serration heights and wavelengths have been tested in conjuction with a highly instrumented NACA 0012 airfoil. It is shown that all serrations cause a significant increase in surface pressure fluctuation spectra in the pre-stall region. However, for angles of attack in the post-stall regime, surface pressure fluctuation spectra reductions of up to 15 dB have been observed for some serrations. These surface pressure fluctuation spectra reductions have been linked to the changes observed in the complex flow-field near the trailing edge, namely boundary layer thickness and velocity fluctuation reductions, as a result of the counter-rotating vortex pairs generated by the respective serrations.

Keywords: Leading Edge Serrations, Separation and Stall Noise, Flow Control, Surface Pressure Fluctuations, Trailing Edge Noise.

1 INTRODUCTION

As the global renewable energy production is increasing rapidly in order to combat man-made climate change, wind turbines are playing a more prominent role. However, concerns have been raised regarding noise emission from wind turbines (1). Brooks *et al.* reported five different airfoil self-noise mechanisms (2), the most relevant for wind turbine noise are trailing edge noise and stall/separation noise. While trailing edge noise and its mitigation has been the subject of a variety studies (2–7), aeroacoustics of separation/stall have received comparably less research attention. Previous experimental studies have found that stall can result in large low-frequency noise and surface pressure spectrum increases (8–10). Stall noise is also hypothesized to significantly contribute to low frequency wind turbine noise, when rapidly changing environmental conditions result in localized stall (11). Recently, leading edge serrations were found to reduce low-frequency stall noise, but increase high-frequency noise (12) and previously, leading edge serrations have been utilized in the field of aeroacoustics to reduce airfoil turbulence interaction noise (13–15). Aerodynamically, leading edge serrations, sometimes also termed leading edge tubercles, have been found to reduce the generated pre-stall lift, while increasing drag for a range of airfoils at moderate Reynolds numbers (16, 17). By contrast, in the post-stall regime, leading edge serration can increase the lift coefficient due to the counter rotating vortices forming over them (16, 17).

This paper aims to experimentally examine the effect of leading edge serrations on the near-field hydrodynamics, especially during stall. Section 2 will introduce the experimental setup, as well as the utilized airfoil and the leading edge serration add-ons, before preliminary surface pressure fluctuation and hot wire results are presented in Section 3. Lastly, Section 4 will provide conclusions and an outlook on future work.

*Ph.D. Researcher Aerospace Engineering, yannick.mayer@bristol.ac.uk.
†Research Associate Aerospace Engineering, nick.zang@bristol.ac.uk.
‡Corresponding Author, Reader in Aeroacoustics, m.azarpeyvand@bristol.ac.uk.

2 EXPERIMENTAL SETUP

2.1 Overview

Experiments were conducted in the aeroacoustic wind tunnel facility of the University of Bristol (18). This study used the larger nozzle with exit dimensions of 500 mm width and 775 mm height at a free stream velocity of $U_\infty = 20\,\mathrm{m\,s^{-1}}$. The nozzle is connected to a test section with tensioned Kevlar windows at the top and bottom, allowing acoustic sound waves to pass through while limiting excessive flow deflection. The angle of attack of the utilized NACA 0012 airfoil with a chord of $c = 300\,\mathrm{mm}$ is controlled by a high torque servo motor as detailed by Mayer *et al.* (19). An overview of the experimental setup and a photo of the NACA 0012 airfoil in the test section is shown in Fig. 1.

The NACA 0012 airfoil is tripped by a zig-zag turbulator trip tape, located at approximately 13 % of the chord on both airfoil sides. The airfoil is equipped with 87 static pressure taps together with 91 embedded microphones placed under 0.4 mm diameter pinholes, namely direct sensing FG-23629-P16 microphones and remote sensing Panasonic WM-61A microphones. All microphones were calibrated in magnitude and phase referenced to a G.R.A.S. 40PL microphone.

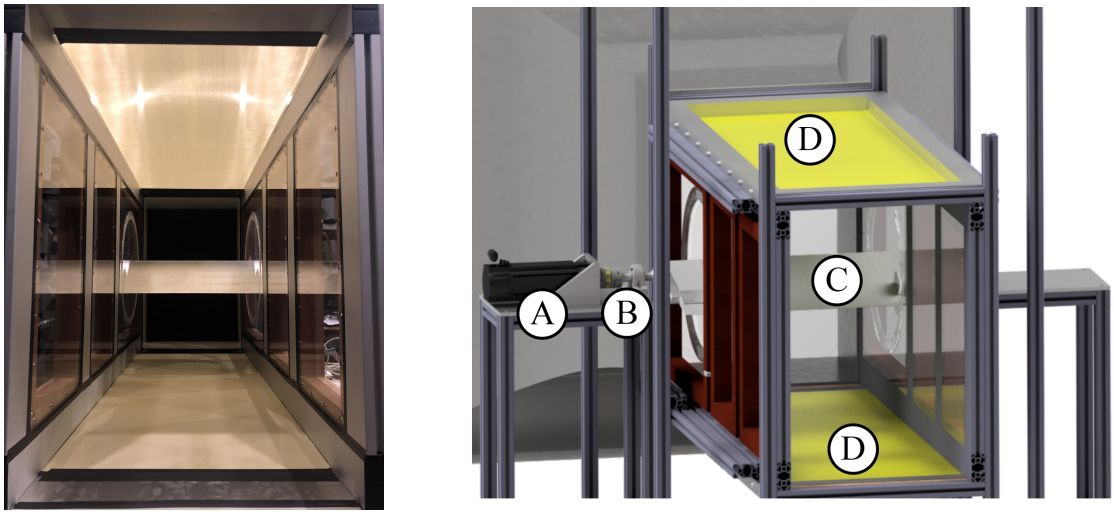

(a) (b)

Figure 1. (a) Upstream view of the test section with the NACA 0012 airfoil installed and (b) Isometric rendering of the experimental setup: (A) servo motor, (B) coupling and bearing, (C) NACA 0012 airfoil and (D) tensioned Kevlar cloth.

2.2 Serration add-ons

Five different leading edge serration add-ons are investigated in this study for varying amplitudes, h, and wavelengths, λ, as detailed in Table 1 and displayed in Fig. 2. The serration add-ons were 3-D printed in polylactic acid material using a dual extrusion Ultimaker 3 printer. All serrations were sanded to provide an aerodynamically smooth surface and since the 3-D printer limited the maximum spanwise serration size, multiple 3-D prints were combined. Aluminium foil tape and polyester flash tape were used to achieve an aerodynamically smooth transition between each individual piece as well as the airfoil and the serrations were tripped consistently with the base airfoil. Variable sized serration pieces on the left and right allowed the serration tip and root plane to be aligned

Table 1. Serration parameters.

No.	h/c_0	λ/h	Designation
1	0.05	1.0	H05Λ10
2	0.10	0.5	H10Λ05
3	0.10	1.0	H10Λ10
4	0.10	2.0	H10Λ20
5	0.15	1.0	H15Λ10

with the chordwise-placed in-situ microphones of the airfoil.

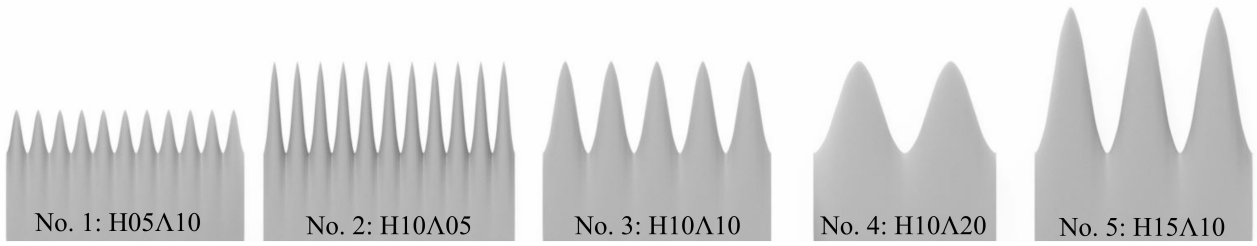

Figure 2. Overview of sections of all serration add-ons used in this study.

The serration add-ons overlap the existing airfoil for 60 mm with a final thickness of 0.4 mm and the mean chord changes sinusoidally in the spanwise direction. Since this study focuses on serration add-ons, the mean chord, c_0, differed for each serration amplitude and was chosen such that the root chord was equal to 305 mm to ease manufacturing of the serration add-ons with sufficient structural integrity. In order to create the chordwise varying serration profiles, the baseline NACA 0012 airfoil profile was scaled along the chord direction.

2.3 Data acquisition and postprocessing

All microphone and hot-wire measurements were sampled simultaneously at a frequency of 2^{15} Hz for 32 s using five 16-channel NI PXIe-4499 modules mounted in a NI PXIe-1062Q chassis. All microphone signals are zero-phase high-pass filtered at 20 Hz, to account for the low-frequency limit of both microphones. A Dantec 55P15 boundary layer hot-wire probe was traversed using two Thorlabs LTS300 stages and operated via a CTA91C10 module. The probe was calibrated daily using a Dantec 54H10 calibrator. The power spectral density (PSD) of the surface pressure fluctuations, ϕ_{pp}, is estimated via Welch's method using a window size of 2^{11} samples and a Hamming window with 50 % overlap, resulting in a frequency bin size of 16 Hz. All surface pressure spectra are normalized with a reference pressure of $p_0 = 20\,\mu$Pa.

3 RESULTS AND DISCUSSION

This section presents surface pressure spectra and boundary layer results for the tip and root plane of all serrations in comparison with the baseline airfoil for different chordwise sensor locations and geometric angles of attack. The baseline airfoil stalls at approximately $\alpha = 14°$ angle of attack (9) and the results are presented for $\alpha = 0°$, $10°$ and $\alpha = 15°$ to investigate the effect of the serrations in different flow regimes.

3.1 Surface pressure fluctuations

Figure 3 shows the surface pressure PSD spectra in the serration tip and root plane at $x/c = 0.43$ for three angles of attack. It is discernible that the difference between the root and tip plane pressure spectra decreases as the angle of attack is increased. At $\alpha = 0°$, the spectra of all serrations differ by no more than 4 dB for all frequencies displayed and for the root plane, the pressure spectra exceed the baseline spectrum by up to 10 dB, while exceeding the baseline spectrum by only up to 3 dB for the tip plane.

The difference between all serrations and the baseline is much more pronounced at $\alpha = 10°$, as the spectra of the serrations exceed the baseline spectrum by up to 25 dB. Additionally, the serration spectra do not peak at 1000 Hz as the baseline case, but rather at frequencies below 200 Hz. Both observations indicate that the flow structures present in the flow have considerably increased in size, which points toward a thicker boundary layer or even flow separation, as serrations can cause earlier stall (16). Increasing the serration amplitude h for $\lambda/h = 1$, leads to an energy increase in frequencies greater than 200 Hz, while at lower frequencies, a serration amplitude of $h/c_0 = 0.1$ results in the lowest surface pressure fluctuations. On the other hand, greater serration wavelengths for an amplitude of $h/c_0 = 0.1$ reveal that the widest serration, H10Λ20, results in the highest surface pressure spectra across the whole frequency range. While H10Λ20 exceeds H10Λ05 by 8 dB at low frequencies, this rises to 25 dB at high frequencies. It is hypothesized that larger and wider serrations induce counter rotating vortex pairs (CVP) with increased vorticity explaining this change. Lastly, it should be mentioned that for the tip plane, a hump between 100 Hz and 300 Hz occurs

for two serrations, namely H15Λ10 and H10Λ20, which could also be caused by the CVP.

Finally, for $\alpha = 15°$, the trends concerning varying serration wavelength and amplitude are almost identical. At low frequencies however, the serrations no longer exceed the baseline spectrum significantly, but are rather below the baseline case, except for the shortest serration, H05Λ10. It is also notable that the shortest serration H05Λ10 has an almost identical surface pressure spectra as the baseline case, suggesting a large degree of similarity between their flow fields.

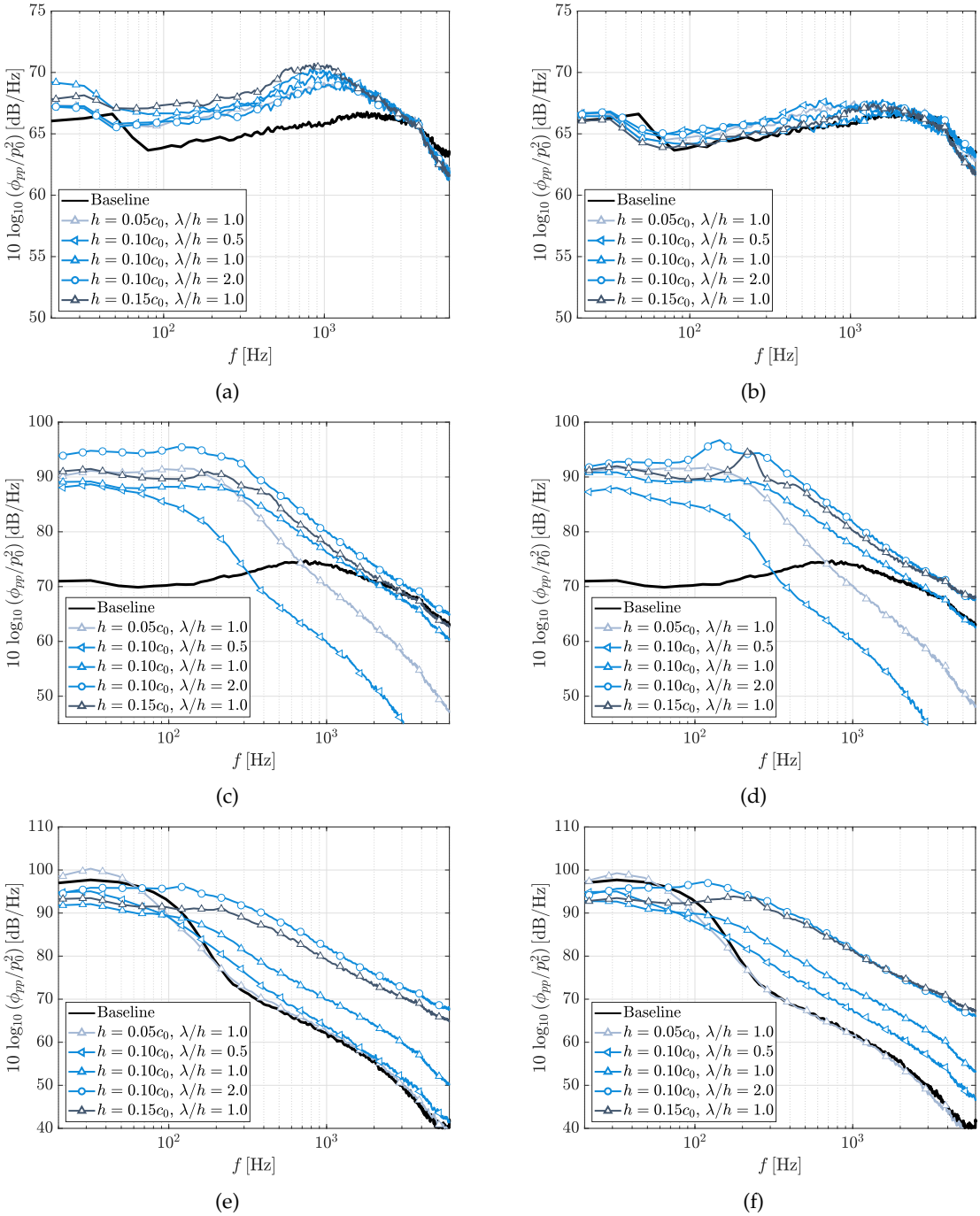

Figure 3. Surface pressure PSD at $x/c = 0.43$: (a) $\alpha = 0°$ root, (b) $\alpha = 0°$ tip, (c) $\alpha = 10°$ root, (d) $\alpha = 10°$ tip, (e) $\alpha = 15°$ root and (f) $\alpha = 15°$ tip.

Figure 4 shows the surface pressure PSD spectra in the serration tip and root plane at $x/c = 0.99$ for $\alpha = 0°$, 10° and 15°. It can be seen that the root and tip plane pressure spectra difference does not exceed 5 dB, and is

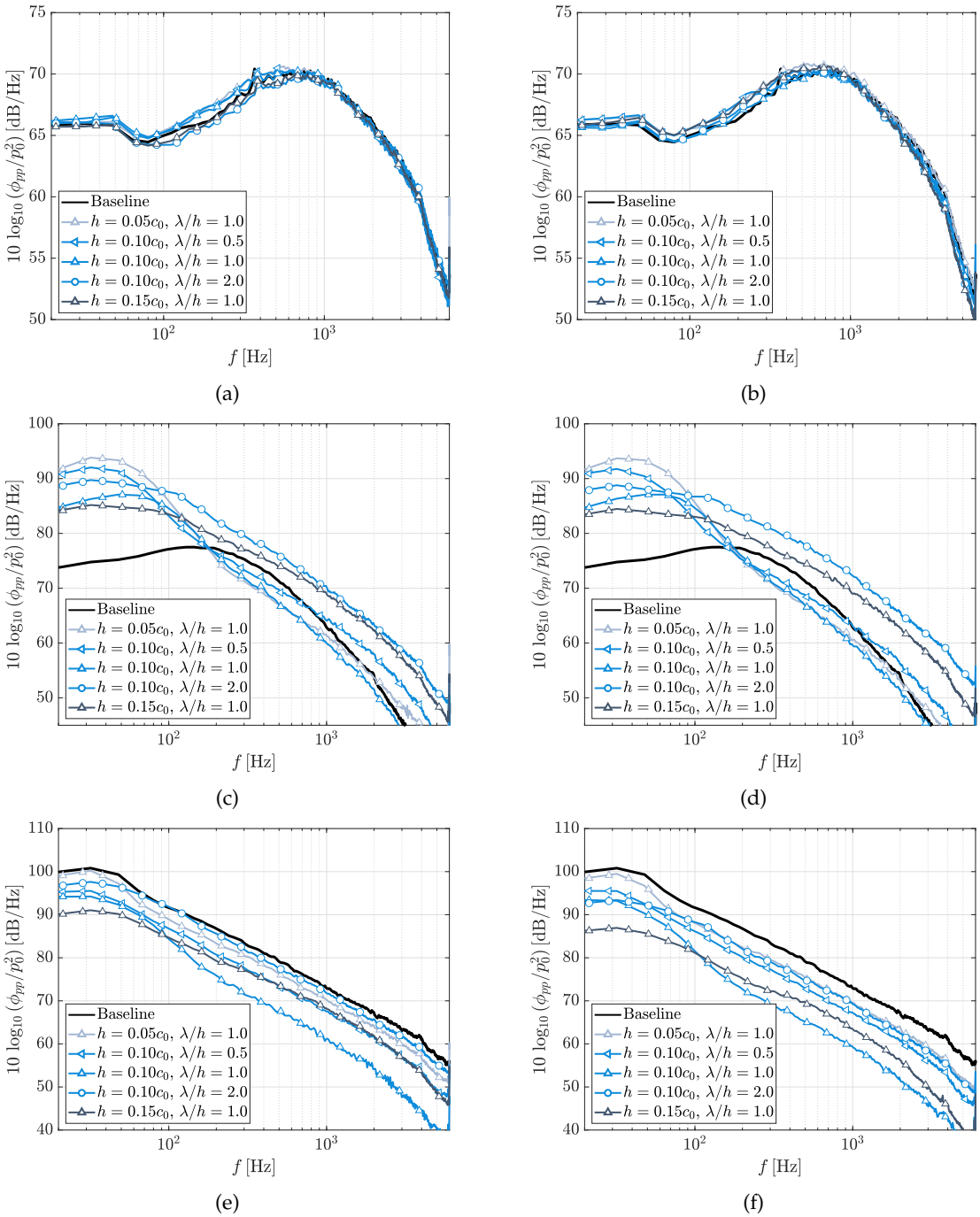

Figure 4. PSD at $x/c = 0.99$: (a) $\alpha = 0°$ root, (b) $\alpha = 0°$ tip, (c) $\alpha = 10°$ root, (d) $\alpha = 10°$ tip, (e) $\alpha = 15°$ root and (f) $\alpha = 15°$ tip.

therefore smaller than at $x/c = 0.43$. This is indicative of a spanwise more homogeneous flow field and hence hydrodynamic pressure field. At $\alpha = 0°$, the spectra of all serrations and the baseline case differ by no more than 2 dB for all frequencies displayed, for both the tip and the root plane.

Again, the difference between all test cases is much more pronounced at $\alpha = 10°$, as the spectra of the serrations exceed the baseline spectrum by up to 20 dB at low frequencies. The peak frequency of the pressure spectra has decreased further compared to $x/c = 0.43$, which is explained by a thicker boundary layer. For a constant serration amplitude of $h/c_0 = 0.1$, the sharpest serration, H10Λ05, possesses the highest low frequency ($f < 200$ Hz) energy and the second highest mid and high frequency energy in comparison to

H10Λ10 and H10Λ20, while H10Λ10 has the lowest energy content. Comparing the results for a constant serration sharpness of $\lambda/h = 1$, it is evident that the longest serration H15Λ10 leads to the lowest low frequency ($f < 100$ Hz) pressure fluctuations, but the highest fluctuations for all other frequencies.

For $\alpha = 15°$, the trends have changed considerably. The pressure fluctuation spectra for all serrations are lower than the baseline spectrum for the complete frequency range displayed. The best performing serration for frequencies below 100 Hz is the longest serration, H15Λ10, exhibiting a reduction of 10 dB. However, for all other frequencies serration H10Λ10 leads to the highest reduction in surface pressure fluctuations, reaching values of up to 15 dB.

3.2 Hot wire results

This section concerns the hot wire measurements conducted near the trailing edge, at $x/c = 0.98$. Figure 5 shows the mean velocity, U, and the velocity fluctuations root-mean-square, U'_{rms}, boundary layer profiles for $\alpha = 0°$, 10° and 15°, normalized with the velocity at the edge of the boundary layer, U_e. For $\alpha = 0°$, all serrations lead to an increased boundary layer thickness and velocity deficit for both the root and the tip plane. Additionally, the outer region of the boundary layer shows an increase in velocity fluctuations for all serrations. These changes confirm the observations from the pressure fluctuation spectra which showed a small increase between the serrations and the baseline case.

However, at $\alpha = 10°$, significant differences are visible in the boundary layer profiles. The boundary layer thicknesses for all serrations exceed the baseline boundary layer thickness by up to 300 % and the boundary layers of the serrations H05Λ10 and H10Λ05 are on the verge of separating. This is a possible explanation for the fact that these two serrations possess the largest low frequency ($f < 100$ Hz) energy in their surface pressure spectra. Similarly, the maximum velocity fluctuations have almost doubled in magnitude for H05Λ10 and H10Λ05, while the other three serrations also display considerable increases, in particular near the airfoil surface. These elevated velocity fluctuations near the surface of the serrations H15Λ10 and H10Λ20, *i.e.* the widest and longest serrations, could offer an explanation for the surface pressure increases at frequencies in excess of 100 Hz for those two serrations. It is assumed that these two serrations both create stronger counter-rotating vortex pairs resulting in a reduced velocity deficit, but greater associated velocity fluctuations.

Finally, for $\alpha = 15°$, the two serrations H05Λ10 and H10Λ05 reveal similarly separated boundary layer velocity profiles as the baseline case, albeit with larger vertical boundary layer separation extents, possibly due to an increased mean chord length. On the other hand, the remaining three serrations have resulted in velocity profiles with comparable boundary layer thicknesses and reduced velocity deficits, which are likely related to stronger CVPs for these larger and wider serrations. Interestingly, the serration with the smallest velocity deficit, H10Λ20, shows the largest near wall velocity fluctuations of all cases up to $y/c = 0.2$, including the baseline case. These velocity fluctuations might explain why this serration has the highest surface pressure spectra of all serrations, except for frequencies below 60 Hz. Lastly, the serrations H10Λ10 and H15Λ10 possess the lowest velocity fluctuations throughout the boundary layer in combination with a reduced boundary layer thickness compared to the baseline case. This ultimately yields the lowest surface pressure fluctuation spectra for these two serrations.

4 FINAL REMARKS

The effect of five leading edge serration add-ons, with various serration heights and wavelengths, on the surface pressure fluctuations and velocity field has been investigated. It is concluded that serrations cause significant increases in surface pressure spectra mid chord, both pre- and post-stall. Similar increases were recorded near the trailing edge, but limited to the pre-stall regime. Post-stall, surface pressure spectra reductions of up to 15 dB have been observed for the serrations H10Λ10 and H15Λ10 and the flow-field results near the trailing edge are consistent with this observation. The serration add-ons are found to cause significant boundary layer thickness increases, prior to reaching the stall angle of attack of the baseline airfoil. Post-stall however, the serrations H10Λ10 and H15Λ10 reduce the boundary layer thickness in combination with smaller velocity fluctuations, compared to the baseline airfoil. The authors therefore hypothesize that serrations require a certain minimum length to be effective in reducing surface pressure fluctuations, and in

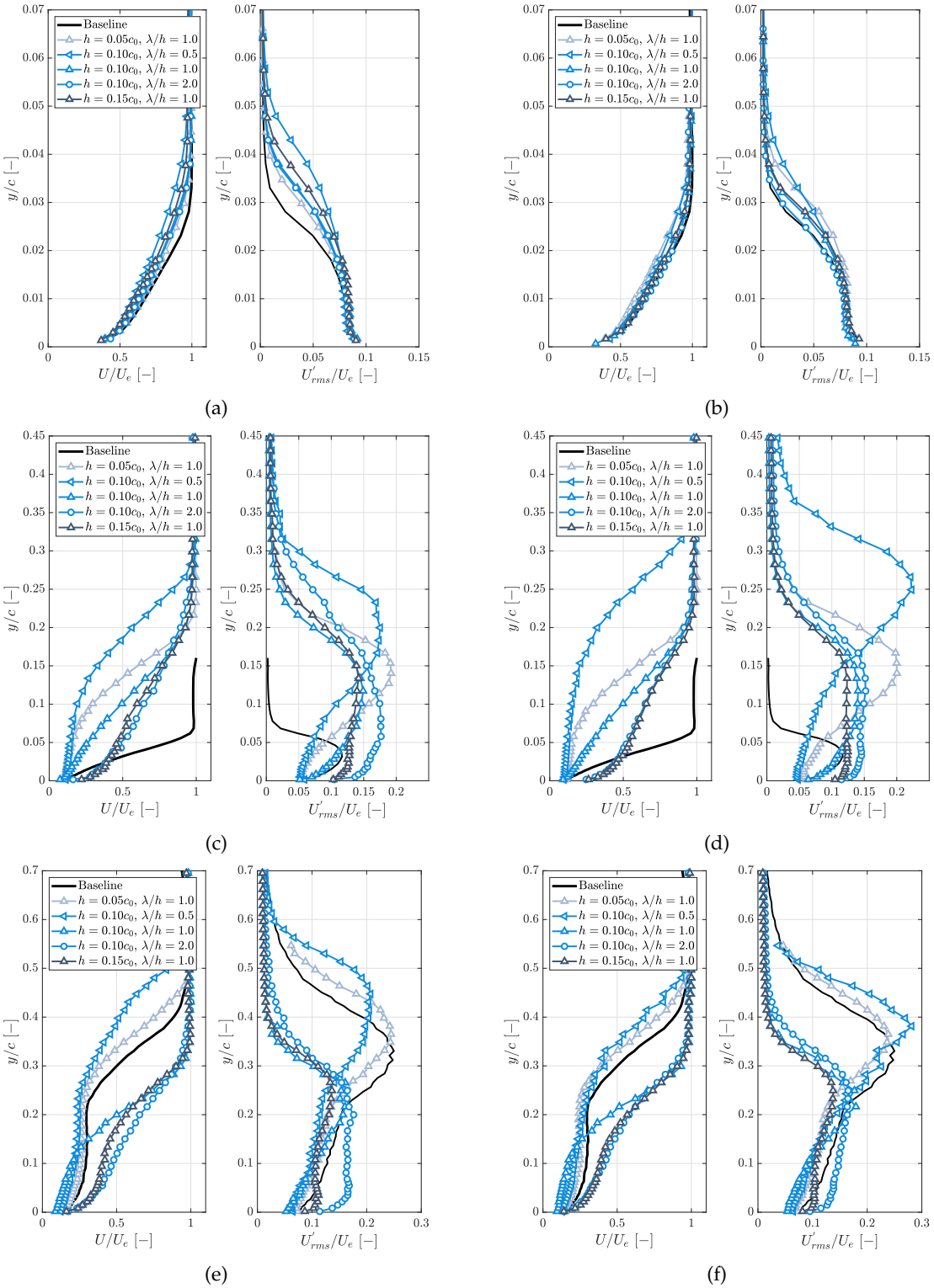

Figure 5. Hot wire measurements at $x/c = 0.98$: (a) $\alpha = 0°$ root, (b) $\alpha = 0°$ tip, (c) $\alpha = 10°$ root, (d) $\alpha = 10°$ tip, (e) $\alpha = 15°$ root and (f) $\alpha = 15°$ tip.

addition, a wavelength-to-serration amplitude ratio near unity appears to reduce surface pressure fluctuations in the post-stall regime.

Most certainly, the complex flow fields caused by different serrations and their effect on the unsteady

surface pressure generation begs further research. Future investigations will take further advantage of the highly instrumented airfoil by investigating the static pressure coefficient, spanwise coherence spectra of the pressure fluctuations and far-field noise measurements. Additionally, surface pressure-velocity field coherence studies will shed further light on the pressure generation regions of the flow field.

ACKNOWLEDGEMENTS

The first author gratefully acknowledges the financial support of the ICA-ASA-DEGA Young Scientists Grant and all authors acknowledge the support of EPSRC (Grant No. EP/R010846/1). Thanks to Pete Coddington for his 3D-printing expertise and to James Filbin and Ben Clark for their help.

REFERENCES

[1] Loren D. Knopper and Christopher A. Ollson. Health effects and wind turbines: A review of the literature. *Environmental Health*, 10(1):78–88, 2011. doi: 10.1186/1476-069X-10-78.

[2] Thomas F. Brooks, D. Stuart Pope, and Michael A. Marcolini. Airfoil Self-Noise and Prediction. Technical report, NASA Langley Research Center, Hampton, Virginia, United States, 1989.

[3] M. S. Howe. A Review of the Theory of Trailing Edge Noise. *Journal of Sound and Vibration*, 61(3):437–465, 1978.

[4] Tze Pei Chong and Alexandros Vathylakis. On the aeroacoustic and flow structures developed on a flat plate with a serrated sawtooth trailing edge. *Journal of Sound and Vibration*, 354:65–90, 2015. doi: 10.1016/j.jsv.2015.05.019.

[5] Yannick D. Mayer, Benshuai Lyu, Hasan Kamliya Jawahar, and Mahdi Azarpeyvand. A semi-analytical noise prediction model for airfoils with serrated trailing edges. *Renewable Energy*, 143:679–691, 2019. doi: 10.1016/j.renene.2019.04.132.

[6] Michaela Herr and Werner Dobrzynski. Experimental Investigations in Low-Noise Trailing-Edge Design. *AIAA Journal*, 46(6):1167–1175, 2005. doi: 10.2514/1.11101.

[7] Mate Szőke, Daniele Fiscaletti, and Mahdi Azerpeyvand. Effect of inclined transverse jets on trailing- edge noise generation. *Physics of Fluids*, 30, 2018. doi: 10.1063/1.5044380.

[8] Stéphane Moreau, Michel Roger, and Julien Christophe. Flow Features and Self-Noise of Airfoils Near Stall or in Stall. In *15th AIAA/CEAS Aeroacoustics Conference*, AIAA 2009-3198, Miami, Florida, United States, 2009.

[9] Yannick D. Mayer, B Zang, and Mahdi Azarpeyvand. Aeroacoustic Characteristics of a NACA 0012 Airfoil for Attached and Stalled Flow Conditions. In *25th AIAA/CEAS Aeroacoustics Conference*, AIAA 2019-2530, Delft, The Netherlands, 2019. doi: 10.2514/6.2019-2530.

[10] Alex Laratro, Maziar Arjomandi, Benjamin Cazzolato, and Richard Kelso. Self-noise of NACA 0012 and NACA 0021 aerofoils at the onset of stall. *International Journal of Aeroacoustics*, 16(3):181–195, 2017.

[11] S Oerlemans. An explanation for enhanced amplitude modulation of wind turbine noise. Technical Report NLR-CR-2011-071, National Aerospace Laboratory, Amsterdam, Netherlands, 2011.

[12] G. Lacagnina, P. Chaitanya, T. Berk, P. Joseph, S. M. Hasheminejad, O. Stalnov, T. P. Chong, and B. Ganapathisubramani. Effect of Leading Edge serrations in reducing aerofoil noise near stall conditions. In *2018 AIAA/CEAS Aeroacoustics Conference*, AIAA 2018-3285, Atlanta, Georgia, United States, 2018. doi: 10.2514/6.2018-3285.

[13] S. Narayanan, P. Chaitanya, S. Haeri, P. Joseph, J. W. Kim, and C. Polacsek. Airfoil noise reductions through leading edge serrations. *Physics of Fluids*, 27(2), 2015. doi: 10.1063/1.4907798.

[14] Auris Juknevicius and Tze Pei Chong. On the leading edge noise and aerodynamics of thin aerofoil subjected to the straight and curved serrations. *Journal of Sound and Vibration*, 425:324–343, 2018. doi: 10.1016/j.jsv.2018.02.038.

[15] B. Lyu and M. Azarpeyvand. On the noise prediction for serrated leading edges. *Journal of Fluid Mechanics*, 826: 205–234, 2017. doi: 10.1017/jfm.2017.429.

[16] Kristy Lee Hansen. *Effect of leading edge tubercles on airfoil performance*. PhD thesis, University of Adelaide, 2012.

[17] H. Johari, C. Henoch, D. Custodio, and A. Levshin. Effects of Leading-Edge Protuberances on Airfoil Performance. *AIAA Journal*, 45(11):2634–2642, 2007. doi: 10.2514/1.28497.

[18] Yannick D. Mayer, Hasan Kamliya Jawahar, Mate Szőke, and Mahdi Azarpeyvand. Design of an Aeroacoustic Wind Tunnel Facility at the University of Bristol. In *2018 AIAA/CEAS Aeroacoustics Conference*, AIAA 2018-3138, Atlanta, Georgia, United States, 2018. doi: 10.2514/6.2018-3138.

[19] Yannick D. Mayer, B. Zang, and Mahdi Azarpeyvand. Design of a Kevlar-Walled Test Section with Dynamic Turntable and Aeroacoustic Investigation of an Oscillating Airfoil. In *25th AIAA/CEAS Aeroacoustics Conference*, AIAA 2019-2464, Delft, The Netherlands, 2019. doi: 10.2514/6.2019-2464.